A MODIFIED SPLIT-STEP FOURIER SCHEME FOR FIBER-OPTIC COMMUNICATION SYSTEM AND ITS APPLICATION TO FORWARD AND BACKWARD PROPAGATION

A MODIFIED SPLIT-STEP FOURIER SCHEME FOR FIBER-OPTIC COMMUNICATION SYSTEM AND ITS APPLICATION TO FORWARD AND BACKWARD PROPAGATION

BY

Xiao Deng, B.Sc.

A THESIS
SUBMITTED TO THE DEPARTMENT OF ELECTRICAL & COMPUTER ENGINEERING
AND THE SCHOOL OF GRADUATE STUDIES
OF MCMASTER UNIVERSITY
IN PARTIAL FULFILLMENT OF THE REQUIREMENTS
FOR THE DEGREE OF
MASTER OF APPLIED SCIENCE

Master of Applied Science (2010) McMaster University
(Electrical & Computer Engineering) Hamilton, Ontario, Canada

TITLE: A modified split-step Fourier scheme for fiber-optic communication system and its application to forward and backward propagation

AUTHOR: Xiao Deng
B.Sc., (Electrical Engineering)
University of Science and Technology of China, Hefei, China

SUPERVISOR: Dr. Shiva Kumar

NUMBER OF PAGES: xi, 57

Abstract

In the passed half century, great improvements have been achieved to make fiber-optic communication systems overweigh other traditional transmission systems such as coaxial systems in many applications. However, the physical features including optic fiber losses, group velocity dispersion (GVD) and nonlinear effects lead to significant system impairments in fiber-optic communications. The nonlinear Schrödinger equation (NLSE) governs the pulse propagation in the nonlinear dispersive media such as an optical fiber. A large number of analytical and numerical techniques can be used to solve this nonlinear partial differential equation (PDE). One of theses techniques that has been extensively used is split-step Fourier scheme (SSFS) which employs the fast Fourier transform (FFT) algorithm to increase the computational speed.

In this thesis, we propose a novel lossless SSF scheme in which the fast decay of the optical field due to fiber losses is separated out using a suitable transformation and the resulting lossless NLSE is solved using the symmetric SSF scheme with some approximations. The various symmetric SSF schemes in terms of accuracy for the given computational cost are compared. Our results show that the proposed scheme

could lead to one or two orders of magnitude reduction in error as compared to the conventional symmetric SSFS when the computational cost is fixed. The proposed scheme can be also used as an effective algorithm for digital backward propagation (BP) too. Our numerical simulation of quadrature amplitude modulation-16 (QAM-16) coherent fiber-optic transmission system with digital BP has shown that the bit error rate (BER) obtained using the proposed scheme is much lower than that obtained using the conventional SSF schemes.

Acknowledgements

I would like to express my most sincere gratitude to my supervisor, Dr. Shiva Kumar, who granted me the opportunity of studying and growing in Canada, gave me his seasoned and patient guidance on my research topic and encouraged me overcoming various obstacles. I also would like to thank Dr. Xun Li who introduced McMaster University to me in 2008 and Dr. Li Yang who gave me important instructions on my research fields during my undergraduate program. The knowledge acquired has allowed me to proceed with this thesis work.

I also would like to thank Dr. Mohamed Bakr and Dr. Xun Li as my defense committee members for taking time in reading, commenting on and evaluating my thesis. The helpful advice will be highly appreciated by me.

I want to appreciate all colleagues of Photonics CAD Laboratory and other friends in both Canada and China for their warm-hearted help and unforgettable friendship.

Last, but not least, I am greatly indebted to my dear parents, grandparents and other family members for their love and support throughout my life. Their continued love and caring has been my spiritual power to face all life challenges on my own.

Contents

List of Figures

List of Abbreviations

PDE	Partial Differential Equation
SMF	Single-Mode Fiber
DFS	Dispersion-Shifted Fiber
WDM	Wavelength-Division Multiplexing
EDFA	Erbium-Doped Fiber Amplifier
OE	Optical-to-Electrical
EO	Electrical-to-Optical
GVD	Group Velocity Dispersion
ISI	InterSymbol Interference
DCF	Dispersion-Compensating Fiber
SNR	Signal-Noise Ratio
NPS	Nonlinear Phase Shift
SPM	Self-Phase Modulation
SSFS	Split-Step Fourier Scheme
FFT	Fast Fourier Transform
FP	Forward Propagation

BP	Backward Propagation
QAM	Quadrature Amplitude Modulation
BER	Bit Error Rate
NLSE	NonLinear Schrödinger Equation
NRZ	Non-Return-to-Zero
PSK	Phase-Shift Keying
ASE	Amplifier Spontaneous Emission
PRBS	Pseudo-Random Bit Sequence
FEC	Forward Error Correction
IXPM	Intrachannel Cross-Phase Modulation
IFWM	Intrachannel Four Wave Mixing

Chapter 1

Introduction

1.1 Evolution of Fiber-optic Communications

During the development of telephone networks in the twentieth century, the use of coaxial cables considerably increased the system capacity. But the frequency-dependent cable losses limited the bandwidth of systems. The short repeater spacing (~km), because of the large cable loss, is also a severe drawback of coaxial-cable systems. Moreover, the bandwidth of the microwave system is limited due to its relatively lower carrier frequency compared with optical communication systems. Optical communication systems use high carrier frequency and the usable bandwidth could be several Tera Hertz. Such systems indeed revolutionized the telecommunication technology and together with opto/microelectronics, led to the advent of the "information age". However, during 1950s, there was neither coherent optical source nor suitable transmission medium. The first problem was overcome in 1960 when the laser was invented. Then a breakthrough occurred in 1970 when the fiber loss is reduced to 20 dB/km near 1 μm wavelength region.

As fiber losses decreasing below 1 dB/km near 1.3 μm wavelength region and InGaAsP semiconductor lasers being developed, the dispersion effects became the major limit to the first generation of fiber-optic communication systems. This problem was overcome by the use of single–mode fiber (SMF) [1] in the second-generation

lightwave systems so that the bit rate reached 1.7 Gb/s and repeater spacing 50 km by 1987.

The drawback of the second-generation lightwave systems described above is the fibers losses near 1.3 μm wavelength region. However, the losses of silica fibers reduced to 0.2 dB/km near 1.55 μm. Thus, using dispersion-shifted fibers (DSF) having minimum dispersion near 1.55 μm or limiting the laser spectrum to a single longitudinal mode could overcome the dispersion problem. The best performance was achieved in combination with theses two approaches leading to 10 Gb/s in 1990 [2]. This is the third-generation lightwave communications.

The fourth generation of lightwave systems introduced the use of optical amplifier for longer repeater spacing and of wavelength-division multiplexing (WDM) for higher bit rate, which resulted in the commercial systems with Tera-Hertz bit rate and 60-80 km repeater spacing.

In the need for higher bit rate, the fifth generation of fiber-optic communication systems attempted to increase capacity and employed erbium-doped fiber amplifier (EDFA) to compensate for fiber losses in optical domain without having to do optical-to-electrical (OE) and electrical-to-optical (EO) conversion in 1989. As the data increases, the dispersion and nonlinearity management of fiber became more and more important.

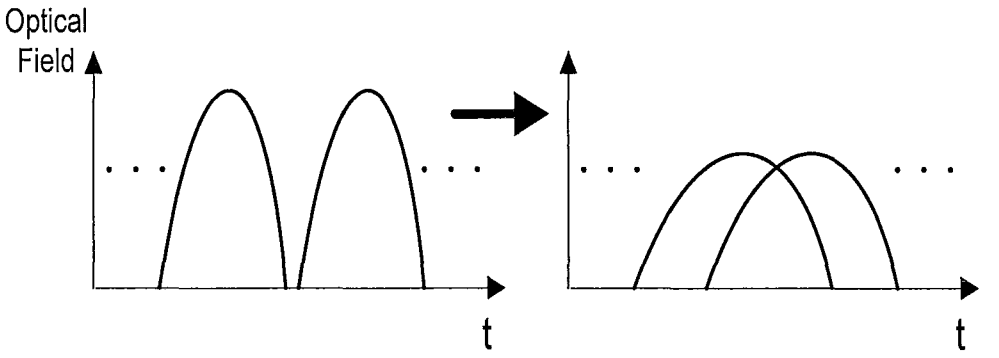

Figure 1. 1: Pulse broadening due to dispersive effect.

1.2 Limitation of Dispersion and Nonlinearity

Group velocity dispersion (GVD) is incurred due to slightly different propagation speeds of different frequency components of pulses. The most direct effect from GVD is broadening of the pulses transmitted. As a result, the pulses overlap as shown in Figure 1.1, resulting in intersymbol interference (ISI). The impact of the dispersion can be conveniently described using the dispersion length defined as [3]

$$L_D = \frac{T_0^2}{|\beta_2|}, \tag{1.1}$$

where T_0 is temporal pulse width and β_2 is the second-order propagation constant. This length provides a scale over which the dispersive effect becomes significant for pulse evolution along a fiber.

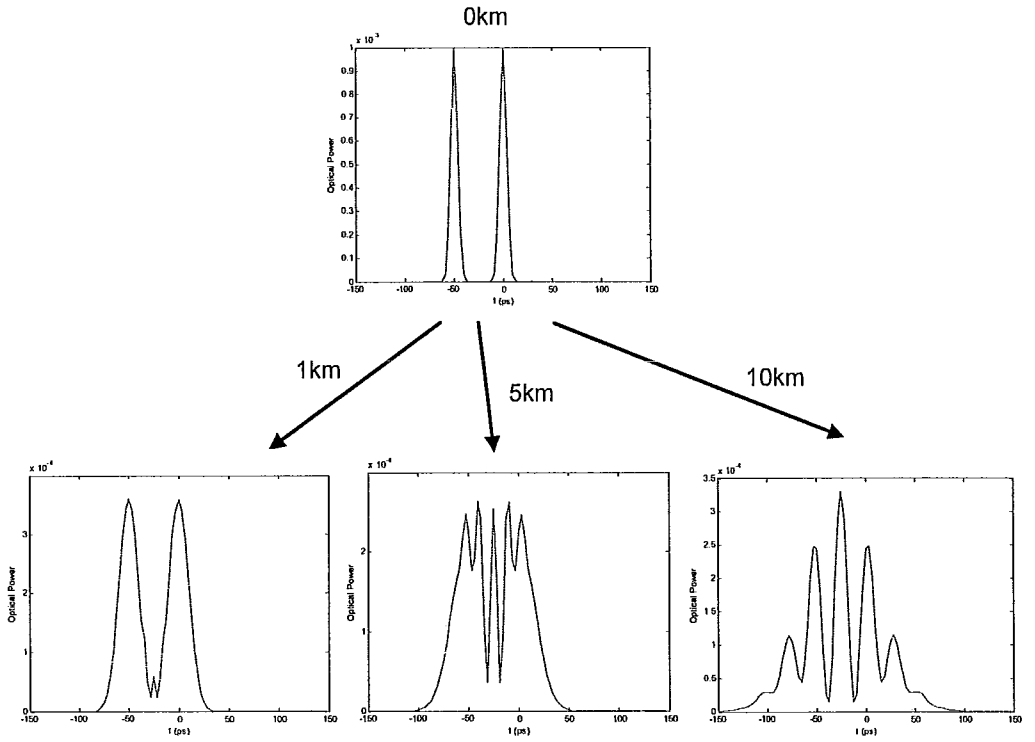

Figure 1. 2: Simulation of dispersive effect on Gaussian pulses broadening.

Assuming the pulse width T_0 equals 10 ps (20 Gb/s 20% Gaussian RZ-OOK) and the second-order propagation constant β_2 is -21 ps^2/km, L_D is approximately 5 km. Over L_D, as Figure 1.2 illustrates, the transmitted pulses are distorted entirely if there is no dispersion compensation. There are several approaches for GVD compensation. Dispersion-compensating fiber (DCF) [4] has the dispersion parameter of an opposite sign with that of the standard transmission fibers. Figure 1.3 shows a fiber optic system using DCF. If the transmission fiber is followed by DCF, total accumulated dispersion is

$$(DL)_{tot} = D_{std}L_{std} + D_{DCF}L_{DCF}, \tag{1.2}$$

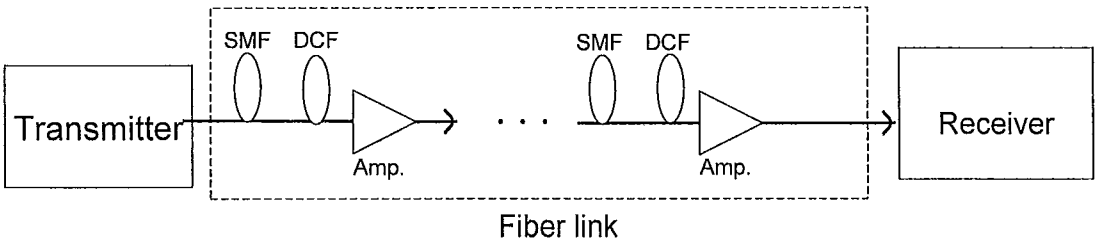

Figure 1. 3: Block diagram of fiber optic transmission system. SMF=Single-mode Fiber and DCF=Dispersion-compensation Fiber.

where D_{std} and D_{DCF} are dispersion coefficients of standard fibers and DCF, respectively, and L_{std} and L_{DCF} are the fiber lengths of the two types of fibers. In principle, adjusting DCF's length, the total accumulated dispersion can be set to zero. For example, the standard fiber has the dispersion coefficient D_{std} with the value of 17 ps/nm/km, and DCF has D_{DCF} with -100 ps/nm/km. So 100 km standard fiber needs 17 km DCF to achieve zero accumulated dispersion.

Another approach is using electronic equalizer at receiving end [5,6] which employs computational algorithms in DSP to compensate dispersive impairments through fibers.

In addition, due to large powers needed to increase signal-noise ratio (SNR), the nonlinear effects in fibers attract more and more attention in modern fiber optic communications. Here, we primarily focus on nonlinear phase shift (NPS) originating from self-phase modulation (SPM). The result of SPM is broadening the spectrum of signals rather than temporal width as GVD does.

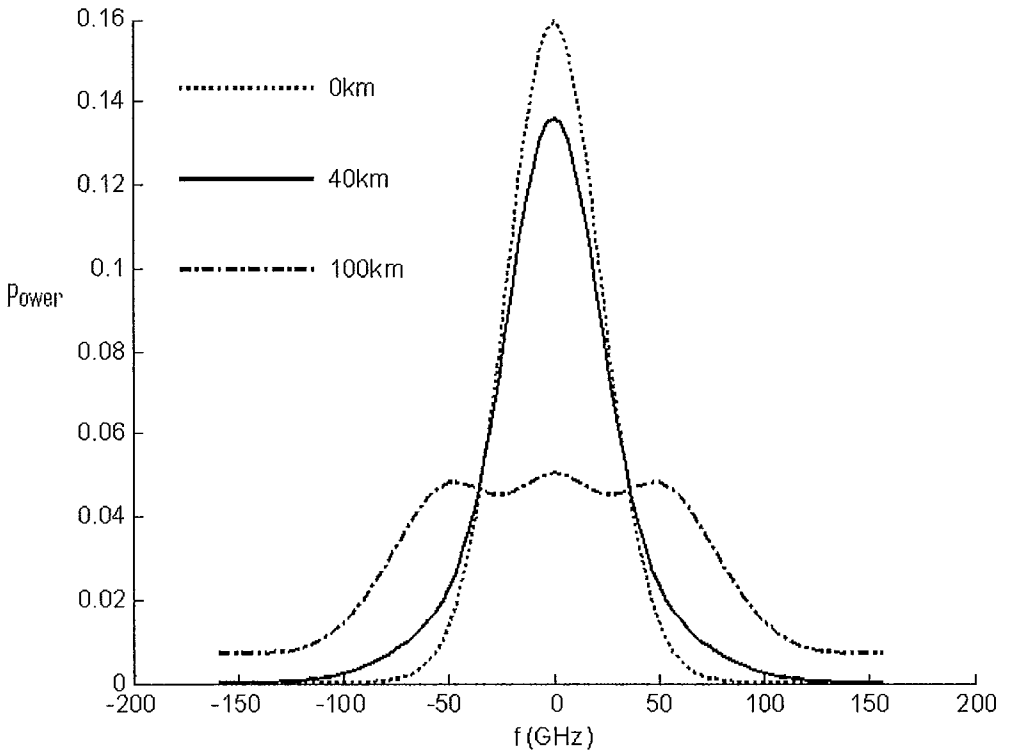

Figure 1.4: Simulation of SPM on spectral broadening.

The mathematical analysis of SPM will be put in Section 2.1. In analogy to dispersion length, a similar concept called nonlinear length is given by

$$L_{NL} = \frac{1}{\gamma P_0}, \tag{1.3}$$

where is γ nonlinearity coefficient and P_0 is launch power. Physically, the nonlinear length indicates the distance at which the nonlinear phase shift reaches to 1 radian. For instance, assume the nonlinearity coefficient γ is 3 $W^{-1}km^{-1}$, the launch power P_0 is 10 mW. So L_{NL} is approximately 30 km, which means that

over 30 km, the spectrum of signals will be broadened to a notable extent. Figure 1.4 shows this clearly.

1.3 Numerical Methods to Solve Nonlinear Schrödinger Equation

Due to the unavailability of analytical solution of the NLSE, a large number of numerical algorithms like the inverse scattering method [7], the finite difference methods [8,9] and the pseudospectral methods [10], can be used to solve this nonlinear partial differential equation problem. The one that has been extensively used is split-step Fourier scheme (SSFS) [11] which employs the fast Fourier transform (FFT) algorithm [12] to increase the computational speed. Typically, the SSFS can be classified into two categories known as the asymmetric SSFS and the symmetrical SSFS. The accuracy of the latter method is one order of magnitude of numerical step size higher than that of the asymmetrical SSFS. The main idea of SSFS is to separate the linear and nonlinear parts of the NLSE. For the linear parts such as dispersion operator, the fast Fourier transform is employed, while with regard to the nonlinear operation, the ordinary differential equation can be solved analytically since in each step size, the nonlinear term is assumed to be constant. This thesis focuses on how the novel technique—the lossless SSFS based on the conventional SSFS is modified, especially the nonlinear operation, to get greater

accuracy in applications of forward propagation (FP) and to obtain better system performances in backward propagation (BP) [13].

1.4 Thesis Structure

This thesis deals with a novel SSFS technique and its simulation and application in fiber-optic communication systems. Chapter 2 introduces the NLSE and explains the conventional numerical methods used to solve the NLSE, especially the conventional split-step Fourier scheme (SSFS). Two topics of the conventional SSFS are discussed and the simulation of fiber-optic system by these techniques is carried out. An error analysis of unsymmetrical and symmetric SSFS shows the advantage of the latter scheme.

In Chapter 3, the lossless SSFS is explained theoretically and schematically. The system structure of the lossless technique used in forward propagation (FP) simulation is illustrated and the results of normalized mean square errors show its advantage compared with other conventional SSFSs.

Chapter 4 shows the system structure of the lossless technique in backward propagation (BP) simulation and the results of bit error rate (BER) indicate that the novel technique saves the computational costs of the receiving-end DSP under the same accuracy as the other conventional SSFS.

Conclusions are drawn and future work is listed in Chapter 5.

Chapter 2

Conventional SSFS used in Solving Nonlinear Schrödinger Equation

2.1 Basic Propagation Equation: Nonlinear Schrödinger Equation

As widely known, Maxwell's equations govern all electromagnetic phenomena with no exception of optical fields. The governing equation that we employed in this thesis for propagation of optical fields in single-mode fibers is the nonlinear Schrödinger equation (NLSE).

In a general form, Maxwell's equations are

$$\nabla \times \mathbf{E} = -\frac{\partial \mathbf{B}}{\partial t}, \tag{2.1}$$

$$\nabla \times \mathbf{H} = \mathbf{J}_f + \frac{\partial \mathbf{D}}{\partial t}, \tag{2.2}$$

$$\nabla \cdot \mathbf{D} = \rho_f, \tag{2.3}$$

$$\nabla \cdot \mathbf{B} = 0, \tag{2.4}$$

where $\mathbf{E}$ and $\mathbf{H}$ are electric and magnetic field vectors, and $\mathbf{D}$ and $\mathbf{B}$ are electric and magnetic flux densities, respectively, which satisfy the relations given by

$$\mathbf{D} = \varepsilon_0 \mathbf{E} + \mathbf{P}, \tag{2.5}$$

$$\mathbf{B} = \mu_0 \mathbf{H} + \mathbf{M}, \tag{2.6}$$

where ε_0 is the vacuum permittivity, μ_0 is the vacuum permeability, $\mathbf{P}$ is the induced electric polarization, and $\mathbf{M}$ is the induced magnetic polarization which is zero in optical fibers. In a medium with no free charges such as optical fibers, the current density vector $\mathbf{J}_f$ and the charge density ρ are required to be zero.

Using Maxwell's equation, it can be shown that the evolution of the optical field envelope in optical fiber is governed by the generalized NLSE [3]:

$$\frac{\partial U}{\partial z}+\frac{\alpha}{2}U+\frac{i}{2}\beta_2\frac{\partial^2 U}{\partial T^2}-\frac{1}{6}\beta_3\frac{\partial^3 U}{\partial T^3}$$

$$=i\gamma\left[|U|^2U+\frac{i}{\omega_0}\frac{\partial}{\partial T}\left(|U|^2U\right)-T_R U\frac{\partial|U|^2}{\partial T}\right], \tag{2.7}$$

where γ is nonlinear coefficient, T_R is related to the slope of the Raman gain, and

$$\beta_n=\left(\frac{d^n\beta}{d\omega^n}\right)_{\omega=\omega_0}, \tag{2.8}$$

For pulses of width T_0 greater than and equal to 1 ps such that $\omega_0 T_0 \gg 1$ and $T_R/T_0 \ll 1$, Eq. (2.7) will be simplified to the NLSE

$$\frac{\partial U}{\partial z}=-\frac{\alpha}{2}U-\frac{i}{2}\beta_2\frac{\partial^2 U}{\partial T^2}+i\gamma|U|^2U, \tag{2.9}$$

where the three terms on the right side denote fiber losses, linear dispersion and low-order nonlinearity, respectively. In this thesis, all analysis and results are based on

Eq. (2.9) that ignores high-order dispersive and nonlinear effects. If only the dispersion considered, Eq. (2.9) can be written as

$$\frac{\partial U}{\partial z} = -\frac{i}{2}\beta_2 \frac{\partial^2 U}{\partial T^2}. \tag{2.10}$$

Taking the FFT of Eq. (2.10), we find

$$i\frac{\partial \widetilde{U}}{\partial z} = -\frac{1}{2}\beta_2 \omega^2 \widetilde{U}, \tag{2.11}$$

where $\widetilde{U}$ is the Fourier transform of U and ω is angular frequency. The solution of Eq. (2.11) is

$$\widetilde{U}(z,\omega) = \widetilde{U}(0,\omega)\exp\left(\frac{i}{2}\beta_2 \omega^2 z\right). \tag{2.12}$$

Thus, the solution of Eq. (2.10) is

$$U(z,T) = \frac{1}{2\pi}\int_{-\infty}^{\infty} \widetilde{U}(0,\omega)\exp\left(\frac{i}{2}\beta_2 \omega^2 z - i\omega T\right) d\omega. \tag{2.13}$$

Let us take a single Gaussian pulse. For example,

$$U(0,T) = \exp\left(-\frac{T^2}{2T_0^2}\right), \tag{2.14}$$

where T_0 is the half-width at $1/\mathrm{e}$-intensity point. Substituting Gaussian pulse to Eq. (2.13), we get

$$U(z,T)=\frac{T_0}{\left(T_0^2-i\beta_2 z\right)^{1/2}}\exp\left(-\frac{T^2}{2\left(T_0^2-i\beta_2 z\right)}\right). \tag{2.15}$$

From Eq. (2.15), it can be seen that the pulse maintain its Gaussian shape but its width at z becomes

$$T'=T_0\sqrt{1+\left(z/L_D\right)^2}, \tag{2.16}$$

where $L_D=T_0^2/|\beta_2|$ is dispersion length. Now, we can see clearly that dispersive effect broadens the pulse and the extent of broadening is scaled by L_D (Figure 1.2).

As with nonlinearity, we consider the equation

$$\frac{\partial U}{\partial z}=i\gamma|U|^2U, \tag{2.17}$$

where γ is nonlinearity coefficient. The solution can be written as

$$U(z,T)=U(0,T)\exp\left(i\phi_{NL}(z,T)\right), \tag{2.17}$$

where the nonlinear phase shift is

$$\phi_{NL}(z,T)=\gamma z\cdot|U(0,T)|^2, \tag{2.18}$$

where $U(0,T)$ is the field amplitude at z=0. If we differentiate the nonlinear phase shift, the frequency difference is obtained

$$\delta\omega(T)=-\frac{\partial\phi_{NL}}{\partial T}=-\gamma z\cdot\frac{\partial|U(0,T)|^2}{\partial T}. \tag{2.19}$$

Eq. (2.19) shows us that new frequency components are generated by SPM to broaden

the spectrum of pulses, and that the time dependence of $\delta\omega$ also leads to frequency chirp.

2.2 The Conventional Split-step Fourier Scheme

The NLSE of Eq. (2.20) is the governing equation to solve the optical field in nonlinear dispersive media like optic fibers. Here the higher-order dispersion and nonlinearity are ignored.

$$\frac{\partial U}{\partial z} = -\frac{i}{2}\beta_2 \frac{\partial^2 U}{\partial z^2} - \frac{1}{2}\alpha U + i\gamma |U|^2 U, \tag{2.20}$$

where U denotes longitudinal envelope of optic field; β_2, α and γ are second-order dispersion parameter, attenuation constant and nonlinear coefficient, respectively. To understand SSFS, the NLSE can be written schematically in the form

$$\frac{\partial U}{\partial z} \triangleq \left(\hat{D} + \hat{\alpha} + \hat{N}\right) U, \tag{2.21}$$

where $\hat{D}$ and $\hat{\alpha}$ are linear operators respectively for second-order dispersion and fiber loss and $\hat{N}$ is a nonlinear operator which is proportional to nonlinear coefficient γ and depends on the local optical power $|U(T,z)|^2$. In mathematical expression, these operators can be shown as

$$\hat{D} = -\frac{i}{2}\beta_2 \frac{\partial^2}{\partial T^2}, \tag{2.22}$$

$$\hat{\alpha} = -\frac{\alpha}{2}, \tag{2.23}$$

$$\hat{N} = i\gamma |U|^2 . \tag{2.24}$$

The analytical solution of Eq. (2.21) is

$$U(z+h) = \exp\left(h\left(\hat{D}+\hat{\alpha}+\hat{N}\right)\right)\cdot U(z), \tag{2.25}$$

where the three operators are carried out simultaneously on the field as one whole operator each step.

In symmetric SSFS, one computing step is divided to two sections, in the middle of which the nonlinearity is lumped. The dispersion operator $\hat{D}$ operates on the field in both sections as explained in Figure 2.1. If the constant operator $\hat{\alpha}$ is combined with $\hat{D}$ as a whole linear operator, the scheme is named as SSFS with loss in linearity, that is, scheme 1. Using the symmetric SSFS and ignoring the terms of the order of h^3 and higher, Eq. (2.25) can be approximated as

$$U(z+h) = \exp\left(\frac{h}{2}\hat{L}\right)\cdot\exp\left(h\hat{N}(z)\right)\cdot\exp\left(\frac{h}{2}\hat{L}\right)\cdot U(z), \tag{2.26}$$

where $\hat{L} = \left(\hat{D}+\hat{\alpha}\right)$. Operator $\exp\left(\frac{h}{2}\hat{L}\right)$ can be implemented numerically, using the fast Fourier transform (FFT).

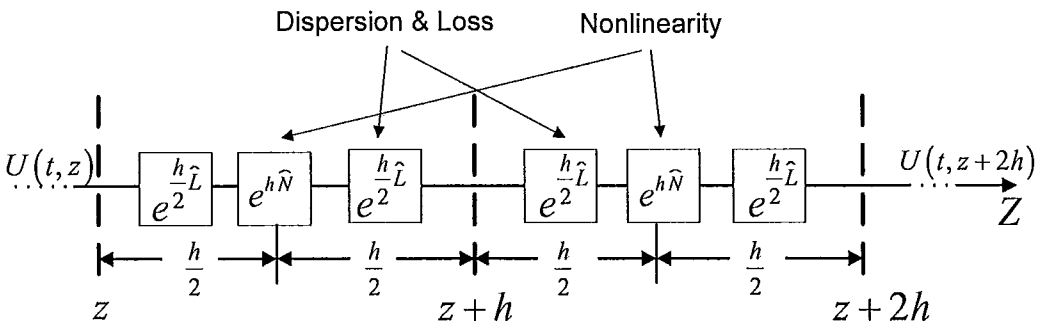

Figure 2. 1: Schematic illustration of symmetric SSF scheme 1.

In Figure 2.2, we show the simulation results using scheme 1 and compare the results between the original input signal and the reference that is SSFS with 0.5 km step size. The simulation system has 100 km long each, 24 fiber spans with 24 amplifiers followed, and at the receiver end, a dispersion compensator is employed to restore the optical waveforms distorted by GVD.

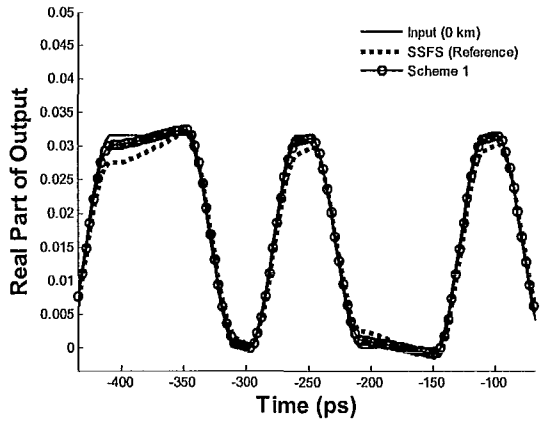

(A)

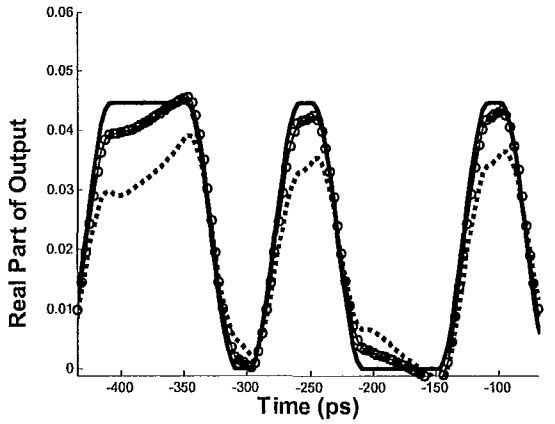

(B)

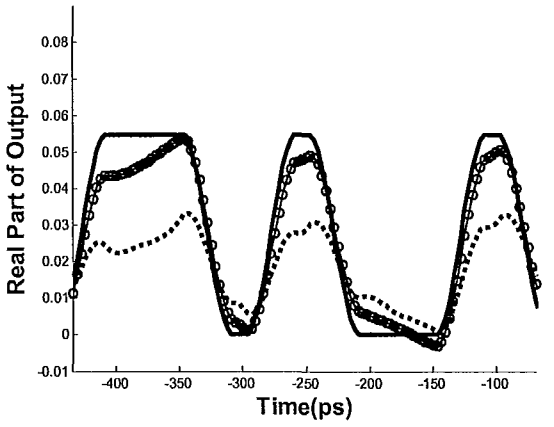

(C)

Figure 2.2: Real part of optical envelope in the case of (A) 1 mW launch power and 2 km step size, (B) 1 mW and 100 km, (C) 10 mW and 100 km for scheme 1.

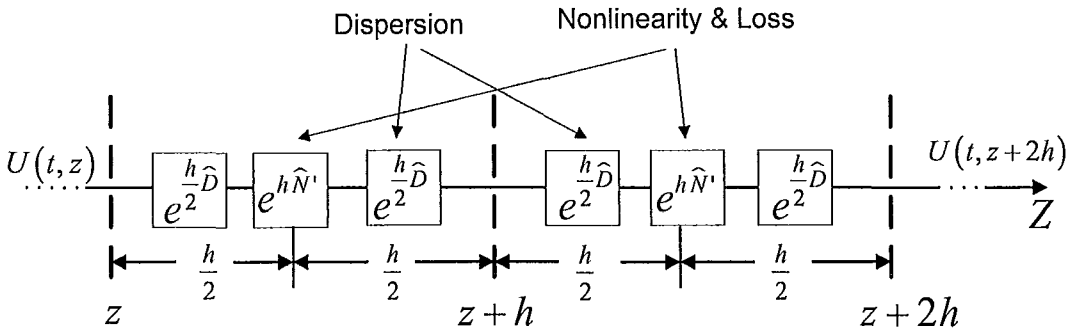

Figure 2.3: Schematic illustration of symmetric SSF scheme 2.

As Figure 2.2 shows, as the step size increasing (Figure 2.2 (A) and (B)), the accuracy of scheme 1 is decreasing compared with reference. Moreover, when the launch power is enhanced, the nonlinearity plays a key role in optical transmission and the pulses (from both reference and scheme 1) are getting distorted, as (B) and (C) in Figure 2.2 show.

Scheme 2, i.e., SSFS with loss in nonlinearity, keeps the similar form of scheme 1 except the position of the loss operator $\hat{\alpha}$:

$$U(z+h)=\exp\left(\frac{h}{2}\hat{D}\right)\cdot\exp\left(h\hat{N}'\right)\cdot\exp\left(\frac{h}{2}\hat{D}\right)\cdot U(z), \qquad (2.27)$$

where the new nonlinear operator $\hat{N}'$ is the addition of $\hat{N}$ and $\hat{\alpha}.$, i.e., $\hat{N}'=\hat{N}+\hat{\alpha}.$ Figure 2.3 illustrates the execution process of scheme 2.

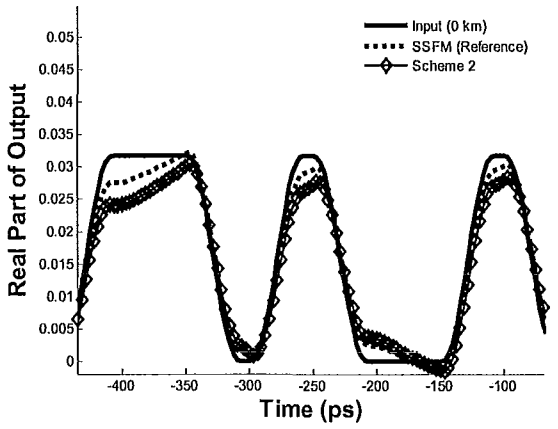

(A)

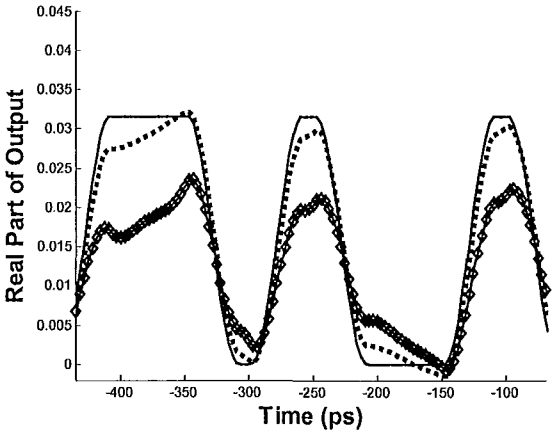

(B)

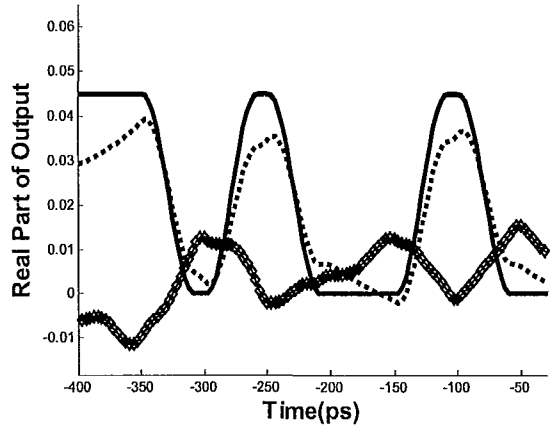

(C)

Figure 2.4: Real part of optical envelope in the case of (A) 1 mW launch power and 2 km step size, (B) 1 mW and 100 km, (C) 10 mW and 100 km for scheme 2.

Figure 2.4 shows the simulation using scheme 2 and compares the results between the original input signal and the reference that is SSFS with 0.5 km step size. The simulation system shares the same frame and parameters as scheme 1. As Figure 2.4 shows, as the step size increasing (Figure 2.4 (A) and (B)), the accuracy of scheme 2 is decreasing compared with reference. Moreover, when the launch power is enhanced, the nonlinearity plays a key role in optical transmission and the pulses (from both reference and scheme 2) are getting distorted (see (B) and (C) in Figure 2.4). Comparing Figure 2.2 (B) and Figure 2.4 (B), we find that the distortion induced in scheme 2 is more than that in scheme 1.

2.3 Error Analysis of Split-step Fourier Scheme

For asymmetric SSFS, the solution is

$$U(z+h,T)=\exp\left(h\widehat{D}\right)\exp\left(h\widehat{N}\right)U(z,T). \tag{2.28}$$

Now set

$$a=h\widehat{D},\ b=h\widehat{N}. \tag{2.29}$$

Use the Baker-Hausdorff formula [14], we obtain that

$$\exp(a)\exp(b)$$

$$=\exp\left\{a+b+\frac{1}{2}[a,b]+\frac{1}{12}[a-b,[a,b]]+\ldots\right\}. \tag{2.30}$$

It is easy to find that the term $\frac{1}{2}[a,b]$ is of second order in h, while the latter term $\frac{1}{12}[a-b,[a,b]]$ is of third order in h that could be neglected. Therefore, the dominant error term is found to result from

$$E=\frac{1}{2}[a,b]=A(T)h^2, \tag{2.31}$$

where

$$A(T)=\hat{D}\hat{N}-\hat{N}\hat{D}. \tag{2.32}$$

Now, set

$$H=a+b=-\frac{i\beta_2 h}{2}\frac{\partial^2}{\partial T^2}+i\gamma h|U_0|^2, \tag{2.33}$$

where the loss operator is left out here for simplicity. According to (2.30), the operator imposed on the input pulse is labeled as

$$\exp\left[h\hat{D}\right]\exp\left[h\hat{N}\right]=\exp[H+E]. \tag{2.34}$$

So, using Taylor expansion, we obtain

$$\exp[H+E]=1+(H+E)+\frac{(H+E)^2}{2!}+\frac{(H+E)^3}{3!}+\ldots$$

$$=\left(1+H+\frac{H^2}{2!}+\frac{H^3}{3!}\right)+[E+\frac{1}{2}(E^2+HE+EH)+\frac{1}{6}(E^3+HE^2+H^2E+EH^2$$

$$+E^2H+HEH+EHE)]+\ldots$$

$$\approx \exp[H]+e, \tag{2.35}$$

where

$$e=[E+\frac{1}{2}(E^2+HE+EH)+\frac{1}{6}(E^3+HE^2+H^2E+EH^2$$

$$+E^2H+HEH+EHE)]+O(h^4). \tag{2.36}$$

Ignoring the third order terms and higher, we obtain the dominant second-order error term in asymmetric SSFS

$$e=A(T)h^2. \tag{2.37}$$

It is worthy to note that the split-step Fourier scheme we are using here is symmetrized as Eq. (2.26) and Eq. (2.27) show. It is concluded that the local error of the symmetric SSFS incurred in a single computation step is proportional to third order of the step size, that is, $O(h^3)$, whereas its error counterpart of asymmetric SSFS has a leading error term of second order. At the meantime, it may appear that the computational cost for symmetric SSFS is more than unsymmetrical SSFS, since $\widehat{D}/2$ should be evaluated twice in a section for symmetric SSFS.

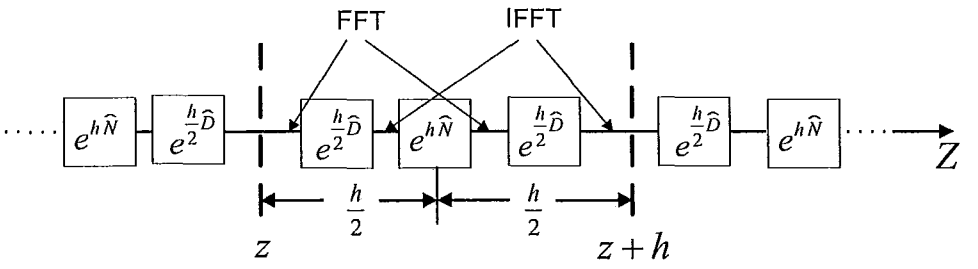

(A)

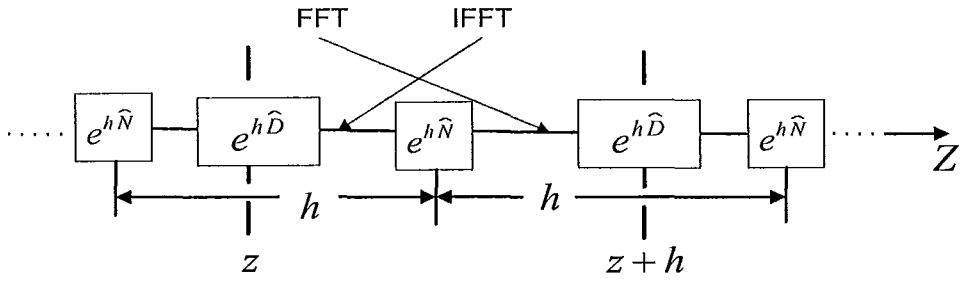

(B)

Figure 2.5: Schematic of symmetric SSFS in (A): original algorithm and in (B): computational simulation in MATLAB.

However, this seeming problem is easily overcome by the technique illustrated in Figure 2.5.

The first half dispersion operation of the current step can be combined with that of the second half of the previous step. Thus, within every step, FFT and inverse FFT are evaluated only once, which is same as that for unsymmetrical SSFS. To summarize, symmetric SSFS can take, with no doubt, the place of the asymmetric scheme with low error and the same computational cost. As follows, we will find out the error and prove it is proportional to h^3.

$$U(z+h,T)=\exp\left(h\widehat{D}\right)\exp\left(h\widehat{N}\right)U(z,T). \tag{2.38}$$

The formally exact solution of Schrödinger equation has been given by Eq. (2.25). For simplicity, we temporarily neglect the loss operator $\widehat{\alpha}$, just keeping the dispersion and nonlinearity operator $\widehat{D}$ and $\widehat{N}$, as Eq. (2.39) shows.

$$U(z+h,T)=\exp\left[h\left(\widehat{D}+\widehat{N}\right)\right]U(z,T). \tag{2.39}$$

For symmetric SSFS, the solution is

$$U(z+h,T)=\exp\left(\frac{h}{2}\widehat{D}\right)\exp\left(h\widehat{N}\right)\exp\left(\frac{h}{2}\widehat{D}\right)U(z,T). \tag{2.40}$$

Now, set

$$a=h\widehat{D},\quad b=h\widehat{N}. \tag{2.41}$$

Use the Baker-Hausdorff formula, and prove Eq. (2.40), we obtain that

$$\exp\left(\frac{a}{2}\right)\exp(b)\exp\left(\frac{a}{2}\right)$$

$$=\exp\left(\frac{a}{2}\right)\exp\left\{b+\frac{a}{2}+\frac{1}{2}\left[b,\frac{a}{2}\right]+\frac{1}{12}\left[b-\frac{a}{2},\left[b,\frac{a}{2}\right]\right]+\ldots\right\}. \tag{2.42}$$

Let us set

$$c=b+\frac{a}{2}+\frac{1}{2}\left[b,\frac{a}{2}\right]+\frac{1}{12}\left[b-\frac{a}{2},\left[b,\frac{a}{2}\right]\right]. \tag{2.43}$$

So, Eq. (2.42) becomes

$$\exp\left(\frac{a}{2}\right)\exp(c)=\exp\left\{\frac{a}{2}+c+\frac{1}{2}\left[\frac{a}{2},c\right]+\frac{1}{12}\left[\frac{a}{2}-c,\left[\frac{a}{2},c\right]\right]\right\}. \quad (2.44)$$

Using

$$\left[b,\frac{a}{2}\right]=\frac{1}{2}ba-\frac{1}{2}ab, \quad (2.45)$$

and

$$\left[b-\frac{a}{2},\left[b,\frac{a}{2}\right]\right]=\frac{1}{2}bba-bab-\frac{1}{2}aba+\frac{1}{4}aab+\frac{1}{4}baa+\frac{1}{2}abb, \quad (2.46)$$

we obtain

$$c=b+\frac{a}{2}+\frac{1}{4}ba-\frac{1}{4}ab+\frac{1}{24}bba-\frac{1}{12}bab-\frac{1}{24}aba+\frac{1}{48}aab+\frac{1}{48}baa+\frac{1}{24}abb, \quad (2.47)$$

$$\left[\frac{a}{2},c\right]=\frac{1}{2}ab-\frac{1}{2}ba+\frac{1}{4}aba-\frac{1}{8}aab-\frac{1}{8}baa+\mathrm{O}\left(h^4\right), \quad (2.48)$$

$$\left[\frac{a}{2}-c,\left[\frac{a}{2},c\right]\right]=\frac{1}{2}bba-\frac{1}{2}bab+\mathrm{O}\left(h^4\right), \quad (2.49)$$

and Eq. (2.3.7) becomes

$$\exp\left(a+b+\frac{1}{12}bba-\frac{1}{8}bab+\frac{1}{12}aba-\frac{1}{24}aab-\frac{1}{24}baa+\frac{1}{24}abb+\ldots\right). \quad (2.50)$$

Therefore, the dominant error term is found to result from

$$E = B(T)h^3, \tag{2.51}$$

where

$$B(T) = \frac{1}{12}\hat{N}\hat{N}\hat{D} - \frac{1}{8}\hat{N}\hat{D}\hat{N} + \frac{1}{12}\hat{D}\hat{N}\hat{D} - \frac{1}{24}\hat{D}\hat{D}\hat{N} - \frac{1}{24}\hat{N}\hat{D}\hat{D} + \frac{1}{24}\hat{D}\hat{N}\hat{N}. \tag{2.52}$$

Let us set

$$\exp\left[h\frac{\hat{D}}{2}\right]\exp\left[h\hat{N}\right]\exp\left[h\frac{\hat{D}}{2}\right] = \exp[H+E]. \tag{2.53}$$

Taylor expansion of the exponential operator on the RHS of Eq. (2.54) leads to

$$\exp[H+E] = 1 + (H+E) + \frac{(H+E)^2}{2!} + \frac{(H+E)^3}{3!} + \ldots$$

$$= \left(1 + H + \frac{H^2}{2!} + \frac{H^3}{3!}\right) + [E + \frac{1}{2}(E^2 + HE + EH) + \frac{1}{6}(E^3 + HE^2 + H^2E + EH^2$$

$$+E^2H + HEH + EHE)] + \ldots$$

$$\approx \exp[H] + e, \tag{2.54}$$

where

$$e = [E + \frac{1}{2}(E^2 + HE + EH) + \frac{1}{6}(E^3 + HE^2 + H^2E + EH^2$$

$$+E^2H + HEH + EHE)] + \mathrm{O}(h^4). \tag{2.55}$$

Here we only considered the terms proportional to h^3, so e is simplified as

$$e = B(T)h^3. \tag{2.56}$$

Comparing Eq. (2.37) and Eq. (2.56), we find that the error is proportional to h^3 in symmetrical SSFS whereas it is proportional to h^2 in asymmetric SSFS.

2.4 Conclusion

After error analysis of the two types of SSFS, the symmetric SSFS possesses an error of third order in h whereas the asymmetric SSFS has a second order error in h. Combining loss operator with dispersion operator, this symmetric SSFS is named as scheme 1. In simulation of NRZ pulses, scheme 1 gives smaller distortion than scheme 2 in which loss operator is combined with nonlinear operator.

Chapter 3

The Novel Lossless Split-step Fourier Scheme And Its Application In Forward Propagation

3.1 Theory of the Lossless Split-step Fourier Scheme

The optical field envelope decreases exponentially with distance due to fiber loss. To separate the rapid change in optical field due to loss, we use the transform

$$U(z,T)=\exp\left(-\frac{\alpha}{2}z\right)\cdot\varphi(z,T). \tag{3.1}$$

By extracting exponential loss, the NLSE governing the new field variable is changed Substituting Eq. (3.1) into Eq. (2.9), we obtain the NLSE in the lossless form

$$\frac{\partial\varphi}{\partial z}=-\frac{i}{2}\beta_2\frac{\partial^2\varphi}{\partial z^2}+i\gamma'|\varphi|^2\varphi, \tag{3.2}$$

where $\gamma'=\gamma\cdot\exp(-\alpha z)$ is the effective nonlinear coefficient that is dependent on z. Eq. (3.2) can be written as

$$\frac{\partial\varphi}{\partial z}\triangleq\left(\hat{D}+\hat{N}_1\right)U, \tag{3.3}$$

where $\hat{N}_1$ denotes $i\gamma'|\varphi|^2$. It can be easily shown that the energy $E=\int|\varphi|^2\,dt$ of the new field φ remains constant as a function of distance z. However, the effective nonlinear coefficient γ' decreases exponentially with distance. In contrast, from Eq. (2.9), it can be shown that the energy $\int|U|^2\,dt$ of the actual field decreases

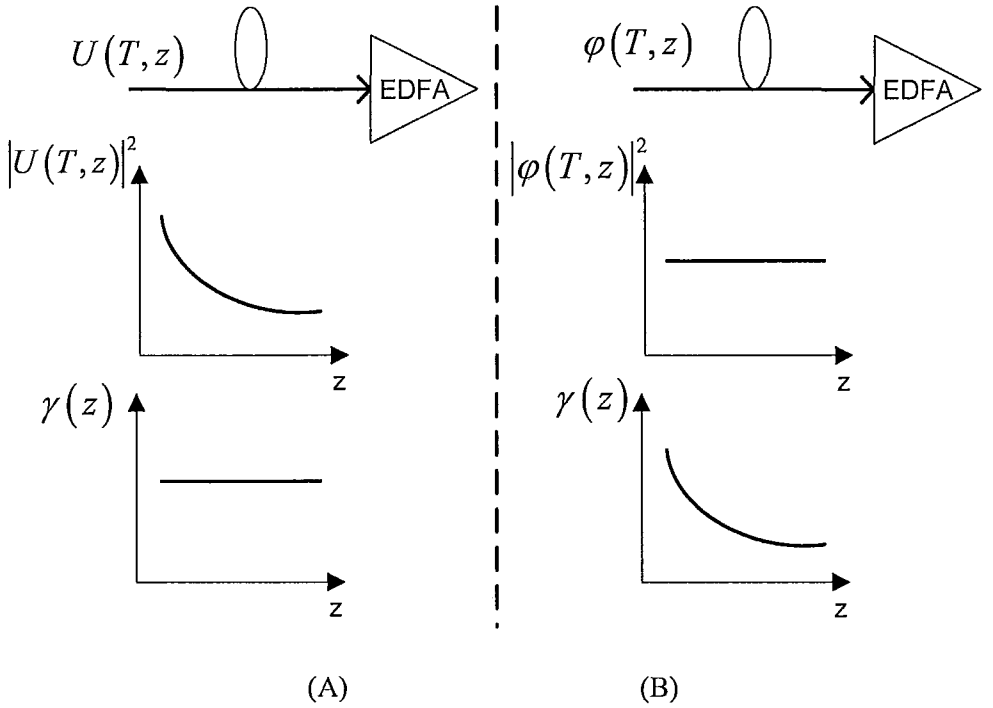

Figure 3.1: Schematic of optical power and nonlinear coefficient in the case of (A) scheme 1,2 and (B) scheme 3.

exponentially with distance, but the nonlinear coefficient remains constant (see Figure 3.1). The allocation scheme of loss and the dependence of nonlinearity on z is the difference between the three schemes and the potential improvement brought by scheme 3. Ignoring the terms of order h^3 and higher, the solution of Eq. (3.3) is given by [3]

$$\varphi(t,z+h)=\exp\left(\frac{h}{2}\widehat{D}\right)\cdot\exp\left[\int_{z}^{z+h}\widehat{N}_1(s)\,ds\right]\cdot\exp\left(\frac{h}{2}\widehat{D}\right)\cdot\varphi(t,z). \qquad (3.4)$$

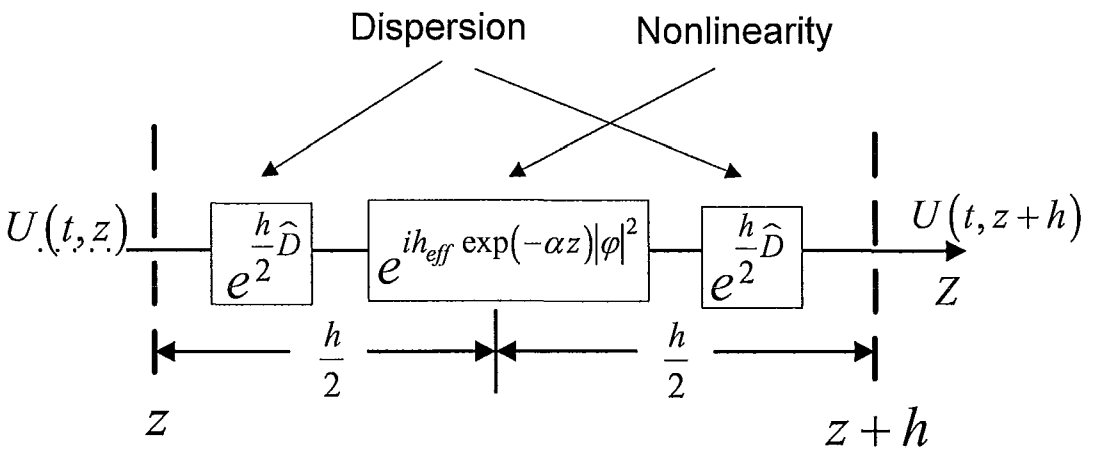

Figure 3.2: Schematic illustration of symmetric SSF scheme 3.

The integral in Eq. (3.4) can be written as

$$\int_z^{z+h} \widehat{N}_1(s)\,ds = i\gamma \int_z^{z+h} \exp(-\alpha s)|\varphi|^2\,ds \tag{3.5}$$

Now, we make an approximation that φ is roughly constant in the interval $[z, z+h]$.

In other words, $|\varphi|^2$ in Eq. (3.5) can be taken out of the integral, i.e.,

$$\int_z^{z+h} \widehat{N}_1(s)\,ds \simeq i\gamma h_{eff} \cdot \exp(-\alpha z) \cdot |\varphi(z)|^2 . \tag{3.6}$$

where

$$h_{eff} = \frac{1-\exp(-\alpha h)}{\alpha}. \tag{3.7}$$

This new scheme is shown in Figure 3.2 and we call it lossless SSFS (scheme 3).

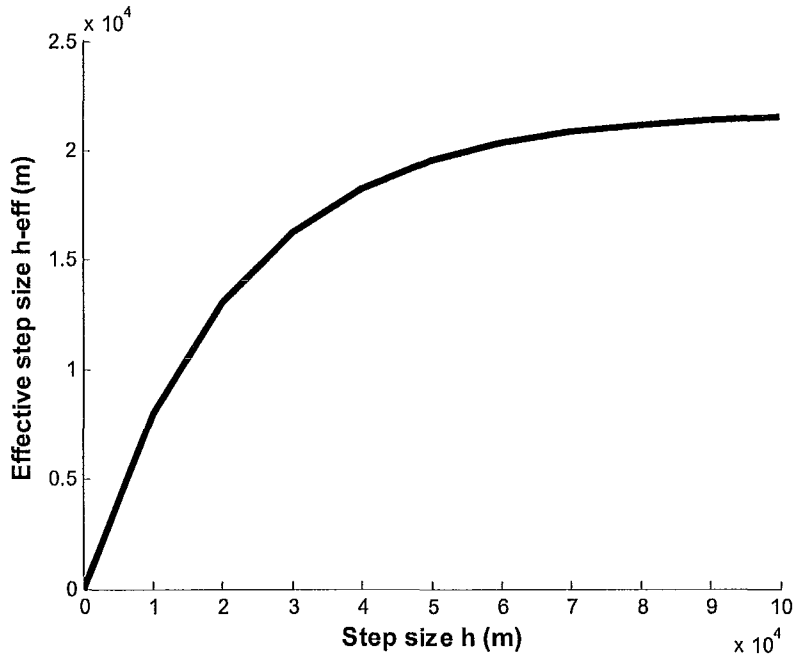

Figure 3.3: Relation of effective step size h-eff and step size h for SSF scheme 3.

Note that when $h \ll 1/\alpha$, $h_{eff} \cong h$, and when $h \gg 1/\alpha$, $h_{eff} \cong 1/\alpha$. Figure 3.3 gives out the relation between h_{eff} and h. From Eq. (2.26), we see that the nonlinear phase accumulated from z to z+h is proportional to h for scheme 1 whereas it is proportional to $h_{eff} \cong 1/\alpha$ when $h \gg 1/\alpha$ for the scheme 3. This implies that larger h can be used for scheme 3 for the given nonlinear phase. Typically, nonlinear phase accumulated over h should be much smaller than π radian and it can be shown that the larger nonlinear phase accumulated over h leads to more errors.

This scheme is advantageous over scheme 1 and scheme 2 for the following reason. For scheme 1, optical power $|U|^2$ decreases exponentially with distance. The nonlinear operator at different computational steps has samples of the exponential

function. When h is large, error increases because of the rapid changes caused by the exponential function. In contrast, in lossless SSFS, the exponential function is analytically integrated as shown in Eq. (3.6), and $|\varphi|^2$ is roughly constant in the interval $[z, z+h]$ because of energy conservation. In next section, we compare the three schemes for forward propagation.

3.2 System Structure Used in Forward Propagation

In this section, we compare the various split-step Fourier schemes for a coherent fiber-optic transmission system shown in Figure 3.4. We assume that the coherent receiver is ideal and ignore the laser phase noise.

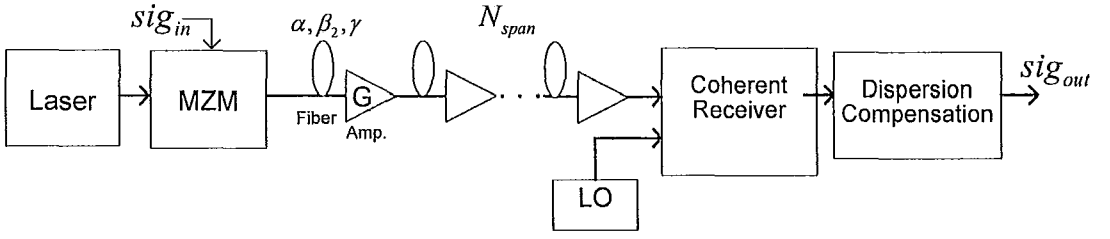

Figure 3.4: Block diagram of a coherent fiber-optic transmission system. MZM=Mach-Zehnder Modulator, Amp.=Amplifier, and LO=Local Oscillator.

The following parameters are assumed: bit rate is set 20 Gb/s, the operating wavelength is 1550 nm, the fiber dispersion coefficient D has the value of 17

ps/nm/km, the fiber loss is equal to 0.2 dB/km and nonlinear coefficient γ is set 1.1 W^{-1} km^{-1}. The laser output is modulated by non-return-to-zero-phase-shift keying (NRZ-PSK) signal using a Mach-Zehnder modulator. The fiber-optic link consists of 24 fiber spans $100\,km$ long each. 24 inline amplifiers compensate the fiber loss exactly. In this section, we turn off the amplifier spontaneous emission (ASE) of the amplifier. A pseudo-random bit sequence (PRBS) with length of 2^{12}-1 is simulated.

3.3 Error Analysis and Method Comparison

To compare various SSF schemes, we define the normalized mean-square error as

$$\bar{e}_{norm} = \int_{-\infty}^{\infty} \left| sig_{i,out}(t, L_{tot}) - sig_{ref,out}(t, L_{tot}) \right|^2 dt \Big/ \int_{-\infty}^{\infty} \left| sig_{ref,out}(t, L_{tot}) \right|^2 dt, \quad (3.8)$$

where $sig_{i,out}$ denotes the output obtained using the SSF scheme i, i=1,2,3, and $sig_{ref,out}$ is the reference output obtained using SSF scheme 1 with very small step size corresponding to a nonlinear phase ϕ_{NL} of 0.0001 radian. For such a small step-size all the three schemes provide the same output.

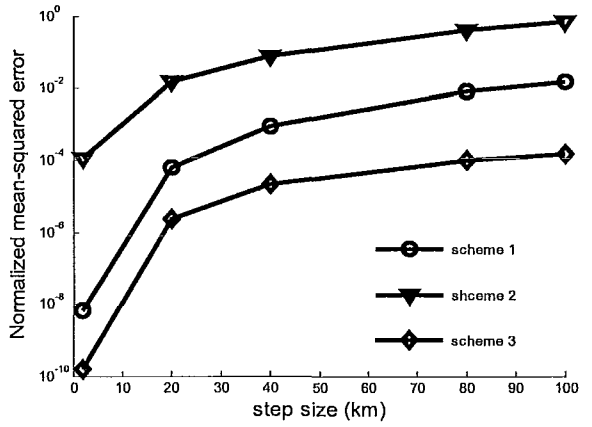
Normalized mean-squared error
step size (km)
scheme 1
shceme 2
scheme 3

(A)

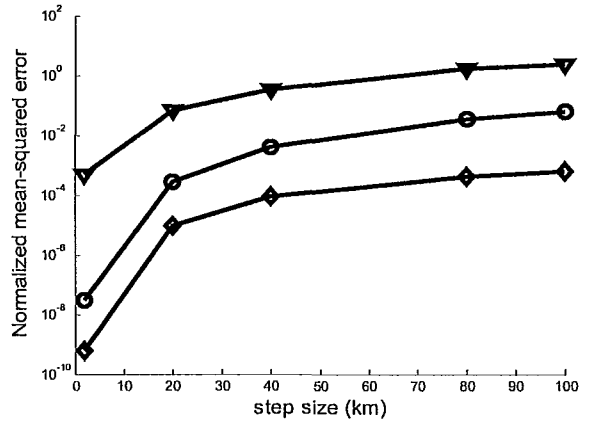
Normalized mean-squared error
step size (km)

(B)

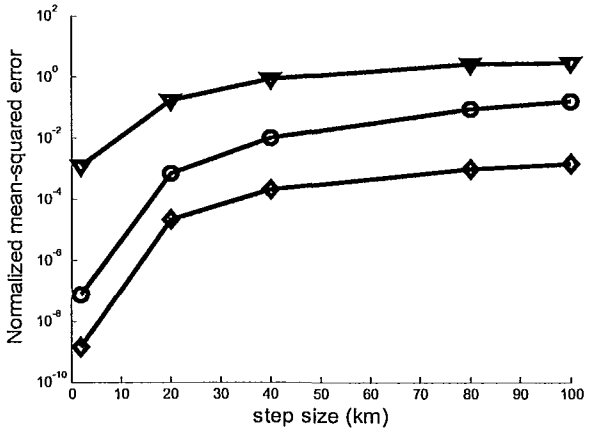
Normalized mean-squared error
step size (km)

(C)

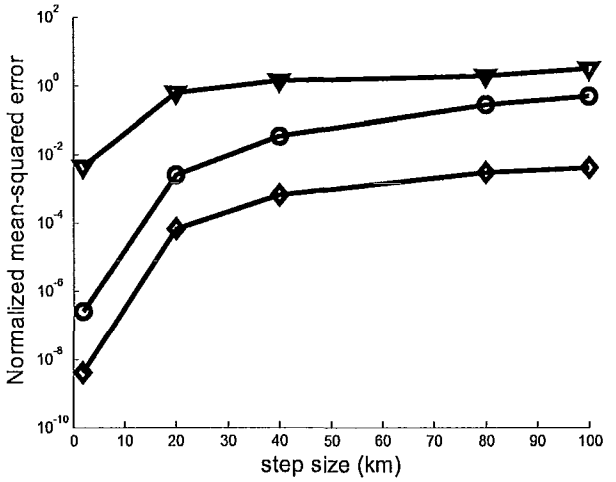

(D)

Figure 3.5: Normalized mean-square errors for raised-cosine NRZ signals in the case of (A) 1 mW, (B) 2 mW, (C) 3 mW and (D) 5 mW launch power over 24×100 km. D=17 ps/nm/km, γ =1.1 W^{-1} km^{-1}.

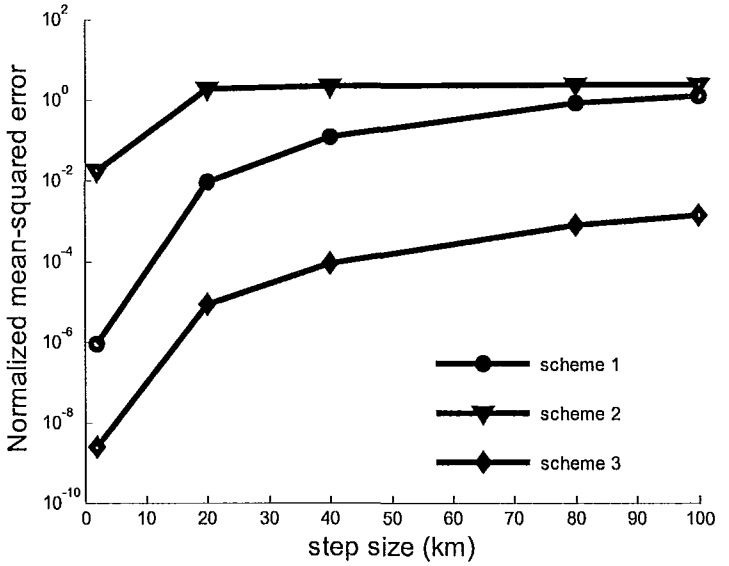

Figure 3.6: Normalized mean-square errors for raised-cosine NRZ signals in the case of 5 mW launch power over 24×100 km. D=2 ps/nm/km, γ =1.1 W^{-1} km^{-1}.

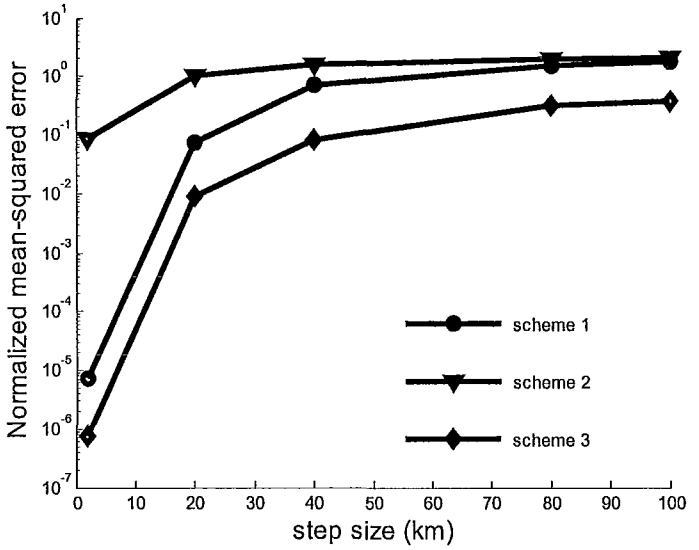

Figure 3.7: Normalized mean-square errors for raised-cosine NRZ signals in the case of 5 mW launch power over 24×100km. D=17 ps/nm/km, γ =2.5 W^{-1} km^{-1}.

Figure 3.5 shows the normalized error as a function of the step size h for various schemes at different launch powers. As can be seen, when the step size is very small, the error is negligible for all the schemes ($e<10^{-2}$). However, when the step size is large, the normalized error for the lossless SSFS (scheme 3) is much lower than the other schemes. In fact, when the step size is 100 km and launch power is 1 mW, the error for the lossless scheme is 100 times lower than scheme 1.

The launch power for Figure 3.6 and Figure 3.7 is 5 mW. In Figure 3.6, dispersion is reduced to 2 ps/nm/km. All other parameters are the same as those in Figure 3.5. In this case we see that, error is 910 times lower than scheme 1 when step size is 100 km. In Figure 3.7, γ is increased to 2.5 W^{-1} km^{-1}. All other parameters

are the same as those in Figure 3.5. Now, we see that the error is 7 times lower than scheme 1 when step size is 100 km.

3.4 Conclusion

Mathematical transformation and approximations make the lossless SSFS (scheme 3) advantageous over the other two conventional SSFSs (scheme 1 and 2). In forward propagation, the novel lossless SSFS gives the least error which is 100 times lower than scheme 1. In the range of relatively large step size (40 km-100 km), the trend of the error curves appears flat, which means that even if the amplifier spacing (100 km) is employed as one step size, the normalized mean squared error is quite small in the examples considered here. A large step size will greatly reduce the running time of computers, especially when a large number of symbols are simulated. In next chapter, we will see its significance in computational cost savings for DSP compensation scheme.

Chapter 4

The Lossless SSFS in Backward Propagation

4.1 System Structure

In direct detection systems, receiver has only the knowledge of the amplitude or power of the received signal, but the phase information is lost. In contrast, in a coherent fiber-optic system, the receiver has the full knowledge of the received field—both amplitude and phase. Therefore, it is possible to avoid the deleterious effects such as dispersion and nonlinearity using digital BP [13]. In digital BP, fiber transmission process is entirely reversed: fiber parameters such as α, β_2 and γ are replaced by a fictitious fiber in digital domain with parameters $-\alpha$, $-\beta_2$ and $-\gamma$, respectively. The amplifier with gain G is replaced by an attenuator with loss 1/G. Typically, the NLSE is solved in electrical (digital) domain with the above parameters using the conventional SSFS. Since computation should be done online, the computational speed should be larger than the symbol rate. Therefore, it is desirable to search for new algorithms that solve the new NLSE faster without losing accuracy. Alternatively, for the given computational cost (or speed), it is desirable to lower the error. In Chapter 3, we have seen that lossless SSFS has the lowest normalized error and therefore, it could be speculated that if the lossless SSFS is used

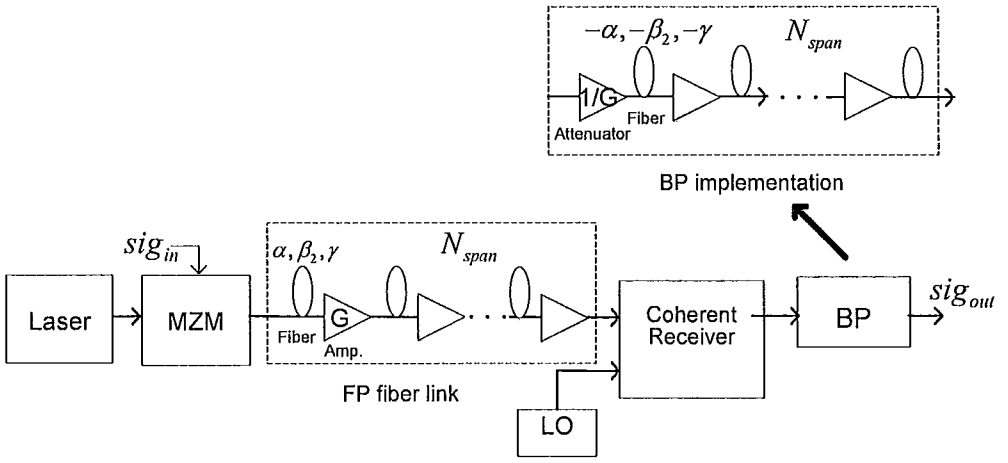

Figure 4.1: Block diagram of BP compensation system. MZM=Mach-Zehnder Modulator, Amp.=Amplifier, LO=Local Oscillator, BP=Backward Propagation.

for digital BP, BER is lowered. To prove this, we have carried out the numerical simulations of the coherent fiber-optic transmission system with the digital BP. A PRBS of length 2^{13}-1 is used to generate QAM-16 data. This data is transmitted over the fiber-optic link described in Chapter 3. At the receiver, digital BP at a symbol rate of 25 GBaud (see Figure 4.1) is used to reverse the effects of dispersion and nonlinearity. An electrical filter with 3 dB bandwidth of 0.2 THz is used. Amplifier ASE is turned on with noise figure 4.8 dB. For the forward propagation, we have used SSF scheme 1 with a nonlinear phase ϕ_{NL} of 0.0001 radian.

4.2 Error Analysis and Method Comparison

For the digital BP, we have used all the three schemes and compared the BER obtained using each of three schemes in Figure 4.2. As can be seen, when the step size is large, the BER is lower by an order of magnitude or more for SSF scheme 3 as compared to scheme 1.

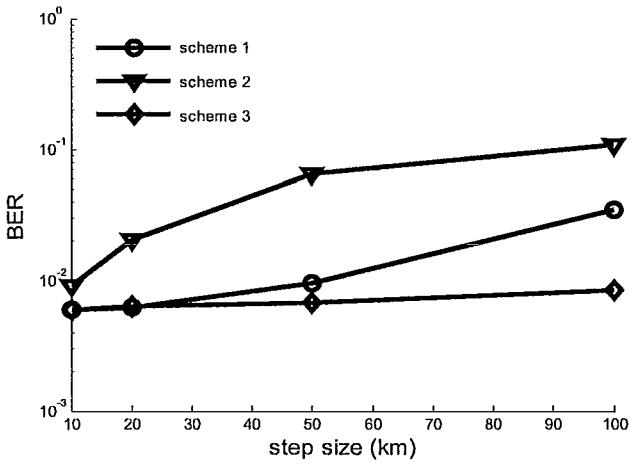
scheme 1
scheme 2
scheme 3
BER
step size (km)

(A)

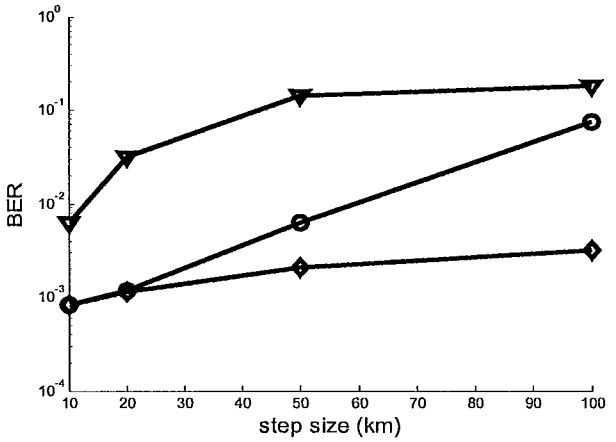
BER
step size (km)

(B)

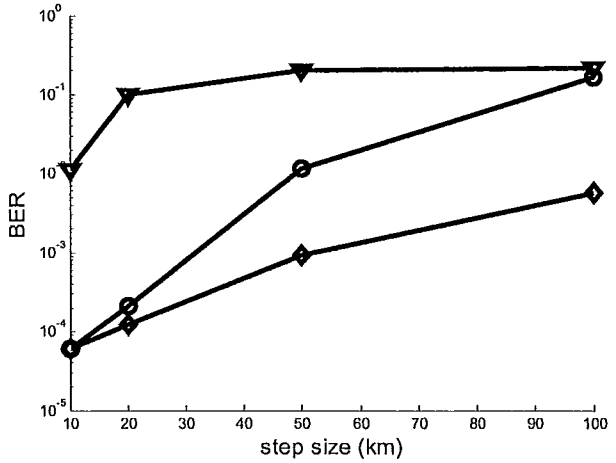
BER
step size (km)

(C)

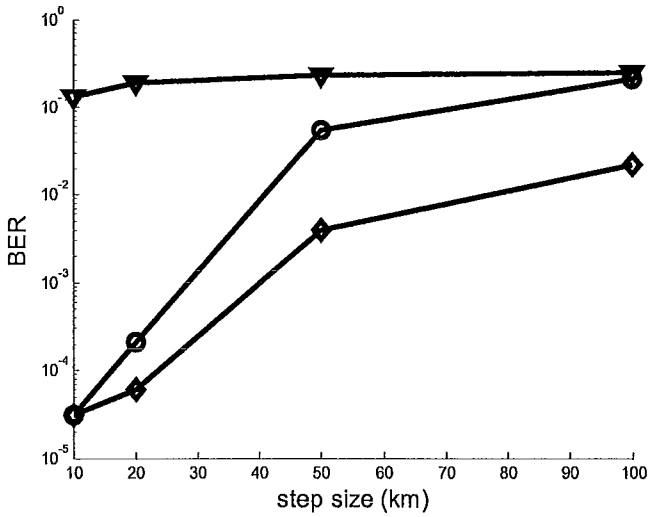

(D)

Figure 4.2: BER along step sizes for 25 Gbaud raised-cosine NRZ-QAM-16 over 14×100 km at launch powers of (A) -3 dBm, (B) -1 dBm, (C) 1 dBm, and (D) 3 dBm.

Figure 4.3 shows the BER vs launch power for various step sizes. When the launch power is very small, the system operates in the linear regime and all the three schemes have the close performance. The performance degradation is caused by the poor SNR. When the launch power is large, the performance is limited by nonlinear effects. When the step size is small (Figure 4.3. (A)), the difference between scheme 2 and scheme 3 is small. However, small step size lowers the computational speed and at larger step sizes (Figure 4.3. (B) and (C)), the optimum BER is significantly lower for the SSF scheme 3. From Figure 4.3. (A)-(C), it can be seen that tolerance to nonlinearity decreases as the step size in digital BP increases.

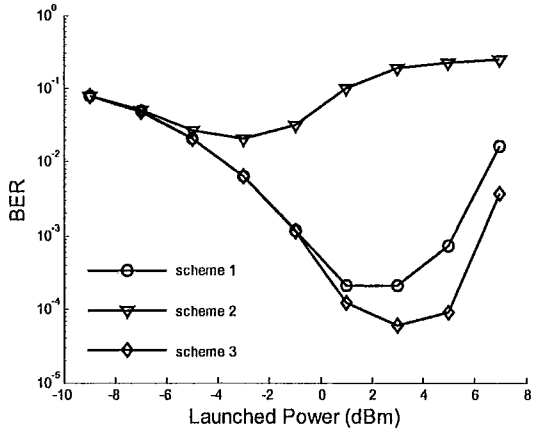

(A)

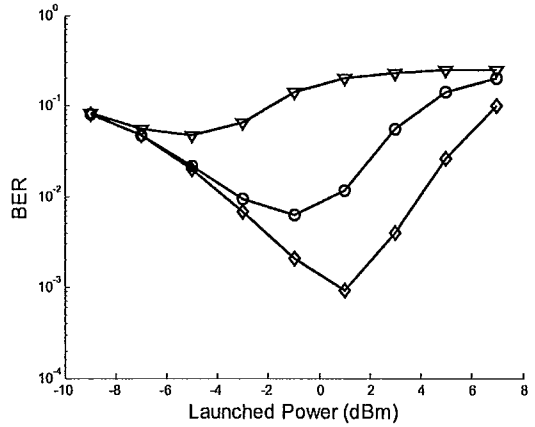

(B)

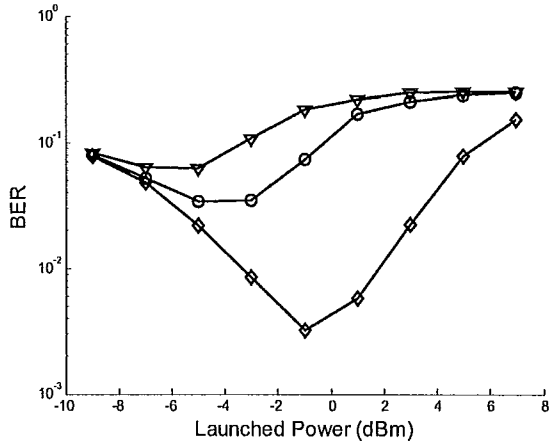

(C)

Figure 4.3: BER vs launch powers at step sizes of (A) 20 km, (B) 50 km and (C) 100 km. Transmission distance=1400 km. D=17 ps/nm/km.

Figure 4.4 also shows the BER vs launch power for various step sizes. But the dispersion parameter D is changed from 17 ps/nm/km to 5 ps/nm/km. The results are qualitatively same as the that shown in Figure 4.3. However, now the transmission distance at which the BER is in the range of 10^{-4} to 10^{-3} is reduced to 600 km from 1400 km. The reduction in transmission reach can be explained as follows: the deterministic nonlinear distortion such as SPM, IXPM and IFWM can be completely undone by the digital BP if the step size is very small (ideal BP). However, the nonlinear interaction between signal and amplifier noise such as that leading to nonlinear phase noise can not be compensated by even ideal BP. It is known that the variance of nonlinear phase noise can be greatly reduced if the fiber dispersion is large [15,16]. Therefore, when dispersion is relatively small (5 ps/nm/km), the nonlinear phase noise becomes the dominant impairment leading to shorter transmission reach.

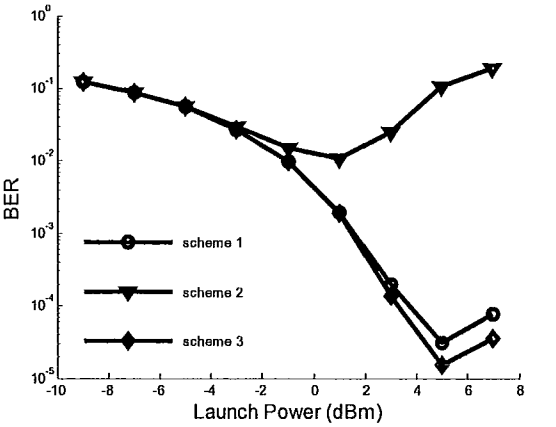

(A)

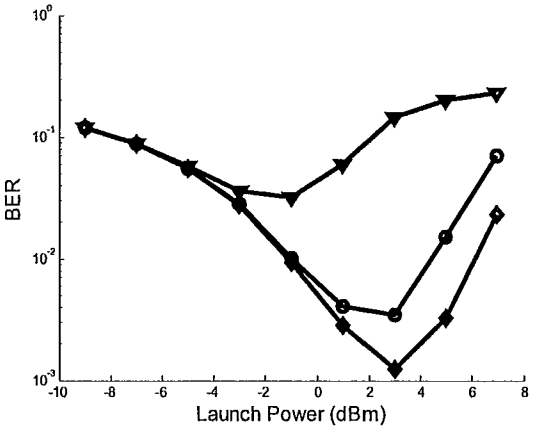

(B)

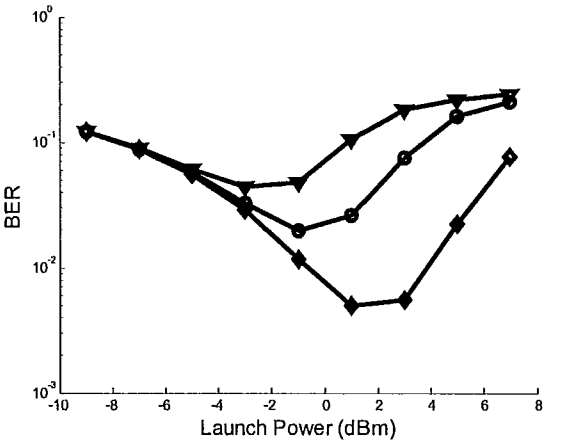

(C)

Figure 4.4: BER vs launch powers at step sizes of (A) 20 km, (B) 50 km and (C) 100 km. Transmission distance=600 km. D=5 ps/nm/km.

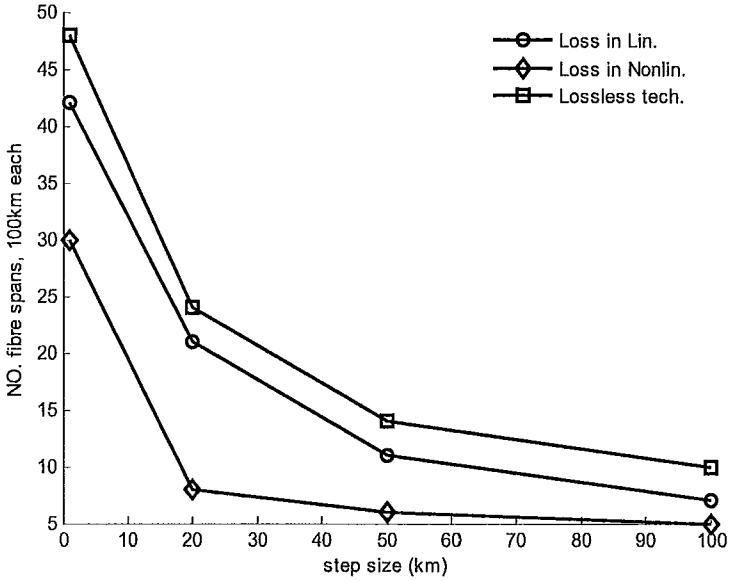

Figure 4.5: N_{span} along step sizes in the case of each method optimized to BER of 2×10^{-3}.

Figure 4.5 shows the number of fiber spans over which the data can be transmitted before the BER reaches the forward error correction (FEC) threshold 2×10^{-3} for the various digital BP schemes. Each span is 100 km-long single-mode fiber. Each point in Figure 4.5 is obtained by optimizing the launch power to the fiber. As can be seen, the transmission reach can be significantly enlarged using the proposed lossless technique.

4.3 Conclusion

In backward propagation, the novel lossless SSFS shows the best system performance and compensates the nonlinear effect more effectively in the range of large launch power. When the computational cost is fixed, we found that the BP using the lossless SSFS technique gives the least BER. Alternatively, to achieve a given BER, lossless SSFS technique has the lowest computational cost.

Chapter 5

Conclusions and Future Work

In this thesis, we have compared two types of SSF schemes in terms of accuracy and speed, and proposed a novel lossless SSFS for the simulation as well as mitigation of nonlinear impairments. The modified lossless SSFS succeeded to achieve better performances in simulation of fiber-optic communication systems. The analytical integration of the nonlinear operator in the new scheme plays the key role in reducing numerical errors. For a 20 Gb/s, NRZ-PSK coherent fiber-optic forward transmission, the normalized mean-square error of the new approach is 100 times lower than scheme 1. Even though at small step size's simulation, the difference of the errors from the three schemes are not clearly big, the modified scheme gives out a better result at large step sizes. As the compensation algorithm to solve inverse NLSE in BP implementation, the lossless SSF scheme provides remarkably lower BER for the 25 GBaud NRZ-QAM-16 coherent fiber-optic communications in contrast to the other conventional SSFSs. Also, in the nonlinear regime at large launch power, the BER obtained from the proposed scheme is lower than that obtained from the other methods indicating the nonlinear impairments can be compensated better using the novel scheme. In this way, the computational overhead of receiving-end DSP will be greatly reduced for the given accuracy.

With regard to the future work, it needs to be seen if the new lossless technique can help when various frequency channels are added in wavelength-division multiplexing (WDM) systems. Moreover, when the step size is made larger than

amplifier spacing, it needs to be seen if the lossless technique is still advantageous over the other conventional SSFSs.

Bibliography

[1] J. I. Yamada, S. Machida and T. Kimura, "2 Gbit/s optical transmission experiments at 1.3 μm with 44 km single-mode fibre," Electron. Lett. **17**, 479 (1981).

[2] G. P. Agrawal, *Fiber-Optic Communication Systems* (John Wiley & Sons, New York, 2002).

[3] G. P. Agrawal, *Nonlinear Fiber Optics* (Academic Press,2001).

[4] P. Palai, R. K. Varshney, and K. Thyagarajan, "A Dispersion Flattening Dispersion Compensating Fiber Design for Broadband Dispersion Compensation," Fiber Integr. Opt., **20**, 21 (2001).

[5] Hyeon-Min Bae, Jonathan B. Ashbrook, Jinji Park, Naresh R. Shanbhag, "An MLSE Receiver for Electronic Dispersion Compensation of OC-192 Fiber Links," IEEE J. Solid-State Circuits, **41**, 2541 (2006).

[6] E. M. Ip, and J. M. Kahn, "Fiber impairment compensation using coherent detection and digital signal processing," J. Lightwave Technol. **28**, 502 (2010).

[7] H. Eichhorn, "Application of the inverse scattering method to the generalized non-linear Schrödinger equation," Inverse Problems **1**, 193-198 (1985).

[8] E. P. Sumesh, and Elizabeth Elias, "Multiwavelet optimized finite difference method to solve nonlinear Schrödinger equation in optical fiber," TENCON 2008 – 2008 IEEE Region 10 Conference, 1-6 (2008).

[9] Sonja Zentner Pilinsku, Zvonimir Šipuš, L'ubomir Šumichrast, "On accuracy of finite-difference method in optical pulse propagation modeling," ICECom 1-3, 274 (2003).

[10] V. E. Zakharov, A. B. Shabat, "Exact theory of two-dimensional self-focusing and one-dimensional self-modulation of waves in nonlinear media," Sov. Phys. JEPT **34**, 62 (1972).

[11] M. Aleshams, A. Zarifkar, M. H. Sheikhi, "Split-step Fourier transform method in modeling of pulse propagation in dispersive nonlinear optical fibers," CAOL 12-17, 124 (2005).

[12] J. W. Cooley, J. W. Tukey, "An algorithm for the machine calculation of complex Fourier series," Math. Comput. **19**, 297 (1965).

[13] Ezra Ip, and Joseph M. Kahn, "Compensation of dispersion and nonlinear impairments using digital backpropagation," J. Lightwave Technol. **26**, 3416 (2008).

[14] Q. Zhang and M. I. Hayee, "Symmetrized split-step Fourier scheme to control global simulation accuracy in fiber-optic communication systems," J. Lightwave Technol. **26**, 302 (2008).

[15] S. Kumar, "Effect of dispersion on nonlinear phase noise in optical transmission systems," Opt. Lett. **30**, 3278 (2005).

[16] A. G. Green, P. P. Mitra and L. G. L. Wegener, "Effect of chromatic dispersion on nonlinear phase noise," Opt. Lett. **28**, 2455 (2003).